Research on Engineering Structures & Materials
www.jresm.org
Research Group

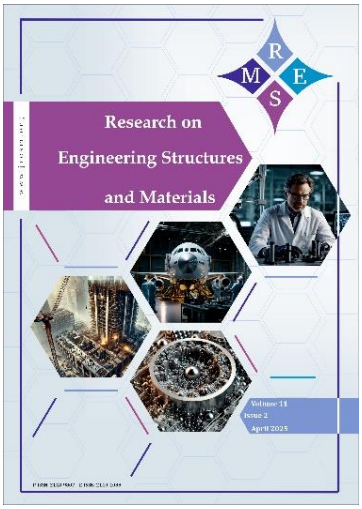

Silica fume-induced phase and structural modifications in biomass-based geopolymer mortars

Andi Yusra, Muhammad Arrie Rafshanjani Amin, Muttaqin Hasan, Husni Husin, Teuku Budi Aulia, Fachruddin Fachruddin, Suryadi Suryadi, Zakia Zakia, Sanusi Sanusi, Lissa Opirina, Andrisman Satria

Online Publication Date: 30 October 2025

URL: http://www.jresm.org/archive/resm2025-1038ma0718rs.html
DOI: http://dx.doi.org/10.17515/resm2025-1038ma0718rs
Journal Abbreviation: *Res. Eng. Struct. Mater.*

To cite this article
Yusra, Amin M A R, Hasan M, Husin H, Aulia T B, Fachruddin F, Suryadi S, Zakia Z, Sanusi Si, Opirina L, Satria A. Silica fume-induced phase and structural modifications in biomass-based geopolymer mortars. *Res. Eng. Struct. Mater.*, 2026; 12(3): 1501-1517.

Research on Engineering Structures & Materials
www.jresm.org

Research Article

Silica fume-induced phase and structural modifications in biomass-based geopolymer mortars

Andi Yusra [*,1,a], Muhammad Arrie Rafshanjani Amin [1,b], Muttaqin Hasan [2,c], Husni Husin [3,d], Teuku Budi Aulia [2,e], Fachruddin Fachruddin [1,f], Suryadi Suryadi [4,g], Zakia Zakia [1,h], Sanusi Sanusi [4,i], Lissa Opirina [1,j], Andrisman Satria [1,k],

[1]*Department of Civil Engineering, Universitas Teuku Umar, Meulaboh, Indonesia*
[2]*Department of Civil Engineering, Universitas Syiah Kuala, Banda Aceh, Indonesia*
[3]*Department of Chemical Engineering, Universitas Syiah Kuala, Banda Aceh, Indonesia*
[4]*Department of Information Technology, Universitas Teuku Umar, Meulaboh, Indonesia*

Article Info

Article History:

Received 18 July 2025
Accepted 28 Oct 2025

Keywords:

Biomass-derived precursors;
Silica fume;
Geopolymer mortar;
Compressive strength;
Microstructure

Abstract

The study explores the influence of silica fume (SF) on the mechanical and microstructural properties of biomass-derived geopolymer mortars. Three pozzolanic precursors rice husk ash (RHA), palm shell ash (PSA), and laterite soil ash (LSA) were combined with SF at substitution levels of 0–20% by binder weight. Alkaline activation employed 6M NaOH and 2.65M sodium silicate. Compressive strength tests, XRD, FTIR, and SEM analyses were conducted. Results showed a substantial strength increase, particularly in RHA-based mortars, from 19 MPa to 52 MPa at 20% SF. XRD and FTIR analyses indicated enhanced gel formation with dominant amorphous phases and stronger Si–O–T and O–H vibrations. SEM images revealed denser microstructures with lower porosity. These findings demonstrate that SF significantly enhances geopolymerization and mechanical performance. The study offers new insights into the use of biomass-derived materials and SF for developing high-performance, sustainable construction mortars.

1. Introduction

Geopolymers are inorganic aluminate-silicate compounds formed through the synthesis of materials rich in silica and alumina, such as FA, RHA, PSA, and various other by-products [1–7]. These materials are activated through alkaline solutions, such as NaOH and Na_2SO_3, which initiate polymerization, resulting in the formation of resilient binding matrices that do not require conventional Portland cement [8,9].

Geopolymer mortar, derived from natural resources, offers a sustainable, cement-free solution that incorporates Industrial by-products abundant in silica and alumina, such as RHA, palm shell ash (PSA), Lokan shell ash (LSA), and silica fume (SF) [10–11]. RHA, rich in amorphous SiO_2, demonstrates significant pozzolanic reactivity, thereby improving the mechanical properties of geopolymer mortars [12]. Likewise, palm shell ash (PSA), which contains reactive silica and alumina, promotes the development of aluminosilicate networks, thereby improving the robustness and longevity of geopolymer mortars establish it as a highly promising sustainable precursor [13,14]. Furthermore, LSA, which contains significant amounts of calcium, contributes to

*Corresponding author: andiyusra@utu.ac.id
[a]orcid.org/0000-0003-4779-0815; [b]orcid.org/0009-0004-1449-7406; [c]orcid.org/0000-0002-8697-912X; [d]orcid.org/0000-0001-8391-119X; [e]orcid.org/0000-0003-1807-1088; [f]orcid.org/0009-0001-1959-8677; [g]orcid.org/0009-0003-3798-8489; [h]orcid.org/0009-0004-5007-9906; [i]orcid.org/0000-0003-2372-9796; [j]orcid.org/0009-0003-4495-9723; [k]orcid.org/0000-0002-8870-9852
DOI: http://dx.doi.org/10.17515/resm2025-1038ma0718rs

facilitates the generation of calcium-aluminosilicate-hydrate (C-A-S-H) gels, gels, thereby improving the performance of geopolymer systems [10,14-16].

The SF a by-product abundant in amorphous SiO_2, significantly enhances geopolymerization Because of its extensive surface area and high chemical reactivity. The added to geopolymer mortars, SF improves the aluminosilicate network formation, which leads to higher compressive strength and overall better performance [15–19]. However, while the individual contributions of various agricultural and marine wastes have been widely studied, few studies have explored the combined use of these wastes along with silica fume in a unified geopolymer system. This gap presents a unique opportunity to assess the synergistic effects of these multi-source precursors in geopolymer mortars. Additionally, shellfish powder, although rich in CaO, provides good workability and rapid setting, but it yields low compressive strength when used alone. In contrast, fly ash offers higher strength but slower setting. A 50:50 blend of fly ash and shellfish powder has been shown to significantly improve strength, suggesting an effective alternative binder that balances performance and reduces the reliance on fly ash [17,20,21].

In this context, the materials used in this study were comprehensively characterized employing XRF, XRD, and FTIR techniques to analyze their chemical composition, crystalline phases, and functional groups. These techniques provided crucial insights into the elemental content, mineralogy, and chemical bonding of the materials, supporting the evaluation of their reactivity, compatibility, and suitability for structural applications [18,22,23]. The alkali activators, particularly the interaction between $NaOH$ and Na_2SiO_3 is essential in driving the geopolymerization process. They facilitate the breakdown of silica and alumina from sources such as LSA, supporting the polycondensation process and the development of a durable aluminosilicate framework [2,24]. The formulation of the alkaline activator solution plays a crucial role in controlling the geopolymerization process, influencing the resulting mechanical strength. This necessitates precise optimization of the component ratios [25–28].

Sodium silicate acts as a chemical accelerator, boosting the reaction rate, improving particle adhesion, and enhancing the cohesion of the geopolymer mortar matrix [23,29]. XRF is used to analyze and quantify the elemental makeup of materials [30–33]. While individual agricultural and marine wastes, along with silica fume, have been investigated in geopolymer systems, limited research has focused on their integrated use within a single geopolymer mortar formulation. This study seeks to fill this gap by exploring the collective impact of RHA, PSA, LSA, and SF in geopolymer mortars. The uniqueness of this study is in examining the combined effect of these multi-source precursors on the mechanical properties and microstructure of geopolymer mortars, aiming to enhance the development of sustainable, high-performance construction materials.

The study is among the few that investigate a hybrid geopolymer system combining agro-based and marine-derived precursors with silica fume in a single formulation, offering a novel approach to enhancing both sustainability and performance in construction materials.

2. Materials and Methods

The study utilized biomass-derived pozzolanic precursors rice husk ash (RHA), palm shell ash (PSA), and Lokan shell ash (LSA) in combination with silica fume (SF) to develop geopolymer mortars. The selection of these materials was based on their high silica and alumina content, confirmed through X-ray fluorescence (XRF) analysis (Table 1), and their local availability as industrial byproducts, aligning with sustainability objectives.

Silica fume was added at substitution levels of 0%, 5%, 10%, 15%, and 20% by binder weight to evaluate its effect on geopolymer performance. Alkaline activation was achieved using a mixture of 6M sodium hydroxide (NaOH) and 2.65M sodium silicate (Na_2SO_3), selected based on previous studies demonstrating optimal reactivity for geopolymerization.

The water-to-binder ratio was fixed at 0.30, balancing workability and mechanical performance. All mortars were cast in 50 mm cube molds and heat treatment (90 °C) for 3 days. For each mix, three specimens were tested for compressive strength, and the average value was reported, with total specimens were 45 pcs. Standard deviation was included to assess data variability.

The mineralogical phases of selected samples were examined using X-ray diffraction (XRD) with a scan range of 5° to 80° (2θ) at a scanning speed of 2°/min. Fourier transform infrared (FTIR) spectroscopy was performed in the range of 400–4000 cm^{-1} with a resolution of 4 cm^{-1}, to analyze functional group changes and gel development. Scanning electron microscopy (SEM) imaging was conducted at magnifications ranging from 500× to 5000× to observe morphological characteristics and microstructural densification.

2.1. Raw Materials

In the research, fine aggregates sourced from KRUENG MEUREUBO were utilized, with a Fineness Modulus (FM) of 2.837%, a bulk density of 1.655 kg/L, a specific gravity of 3.14, a water absorption rate of 1.837%, and a sediment content of 4.75%. Lokan shell ash was used as the main precursor, with silica fume added at varying levels of 0%, 5%, 10%, 15%, and 20% by the weight of the precursor. The alkaline solution consisted of a 1:1 ratio of NaOH and Na_2SO_3, with NaOH having a molarity of 6 M and Na_2SO_3 at 2.65 M. Aggregates, crucial as filler materials in concrete and mortar, significantly impact their composition and performance. Typically, they constitute 70% to 75% of the total volume in hardened mortar, influencing the material's overall quality. Therefore, selecting appropriate aggregates is vital for optimizing the performance and durability of concrete [34]. The alkaline activator comprised a 1:1 ratio of NaOH (6 M) and Natrium silicate (2.65 M) solutions [35].

A range of agricultural and marine waste-derived materials were utilized as aluminosilicate precursors in the production of geopolymer mortars. These materials, including RHA, PSA, LSA, and silica fume (SF), were chosen for their pozzolanic properties and chemical compositions, which are favorable for the geopolymerization process.

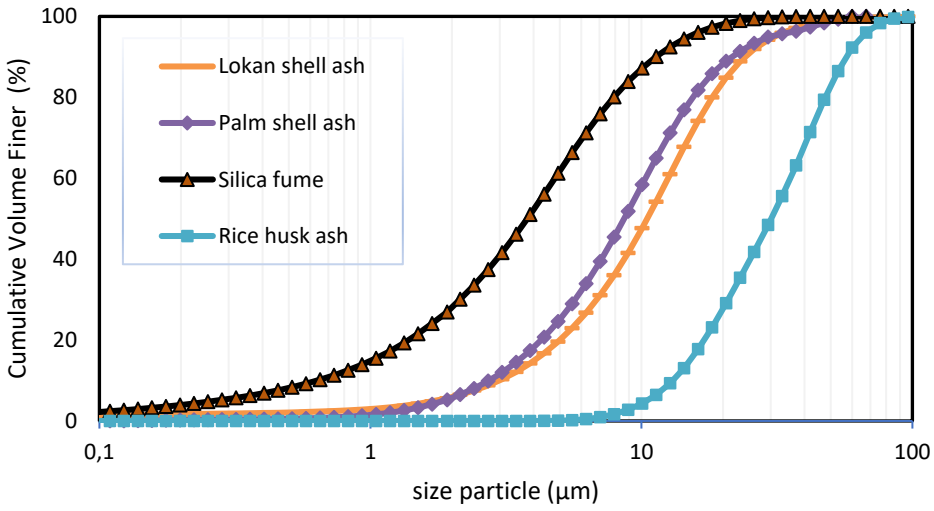

Fig. 1. Graph of the distribution of Binder and Silica Fume materials

Fig. 1. presents the particle size distribution of the aggregate, in accordance with the SNI-03-2847-2002 standards. It includes curves for the upper limit (maximum fine content), intermediate zones (well-graded distributions for optimal packing density), and lower limit (minimum fine content). The dotted line represents the gradation used in this study, which lies within the permissible range, indicating a balanced selection of fine and coarse fractions to optimize mortar performance. This gradation confirms compliance with standard specifications and ensures structural adequacy.

2.1.1. XRF

XRF is used to analyze and quantify the elemental composition of materials. In cementitious systems, SiO_2 and Al_2O_3 enhance mechanical strength, while CaO influences workability and setting of fresh mixtures. Figure 2 displays the XRF spectrum of the LSA binder, highlighting silica (SiO_2) as the dominant component, with significant amounts of CaO and Fe_2O_3, indicating potential C–A–S–H synthesis and thermal stability. Minor elements (Mg, K, Na, Al) and trace levels of Cl, P, Ti, and S suggest a complex mineral composition contributing to the binder's reactivity.

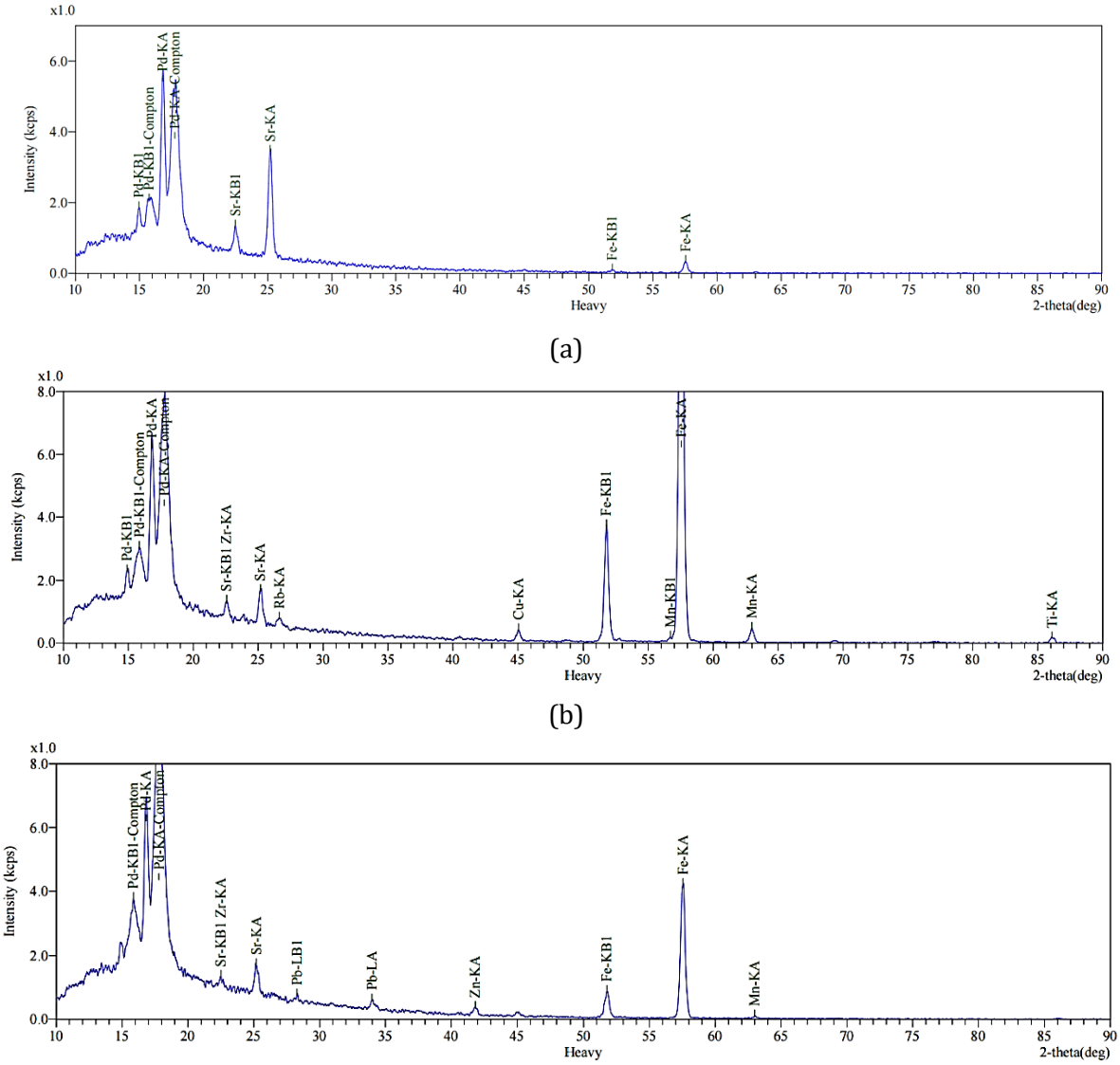

Fig. 2. X-ray fluorescence (XRF) spectrum of RHA, LSA and PSA

Figure. 2.a displays of XRF spectrum of RHA, with silica (SiO_2) identified as the primary component, accompanied by significant quantities of K, Ca, and P. Trace amounts of Al, Mg, Na, Fe, as well as minor elements like Zn, Mn, and Cl, reflect the complex composition of RHA. The high SiO_2 content underscores its potential as a reactive pozzolanic material for both geopolymer and cementitious applications.

Table 1 summarizes the functional properties of RHA, highlighting its high amorphous silica content as the key contributor to pozzolanic reactivity and aluminosilicate gel formation, which enhances strength and durability. Minor components such as CaO, Al_2O_3, K_2O, and Na_2O support additional gel phase formation and early geopolymerization, positioning RHA as an effective supplementary precursor for sustainable, high-performance binders. The outlines the functional role of LSA in geopolymer systems, emphasizing SiO_2 as the main pozzolanic component and CaO as an essential element in the development of C–A–S–H, enhancing early strength. Fe_2O_3 improves thermal stability and reactivity, while Al_2O_3 and MgO support matrix stability and phase development. Trace oxides (Na_2O, K_2O, SO_3) may act as activators, promoting early geopolymerization and influencing phase assemblage. The outlines the functional performance of PSA, highlighting its high SiO_2 and CaO content as key contributors to pozzolanic reactivity. Fe_2O_3 enhances chemical reactivity, while Al_2O_3 and MgO support phase development and hydration. Minor oxides (Na_2O, K_2O) act as fluxes or accelerators, and trace components (ZnO, Cr_2O_3, P_2O_5,

SO_3) may influence stability, redox behavior, and sulphate resistance. This multi-oxide composition affirms PSA's suitability as a pozzolanic precursor for high-performance geopolymer binders.

Table 1. presents an overview of the chemical composition of binder.

Binder	Element	Relative Intensity	Chemical Compound
RHA	K	Low	K_2O
	Ca	High	CaO
	P	-	P_2O_5
	Al	Low	Al_2O_3
	Mg	Low	MgO
	Na	Low	Na_2O
	Fe	Moderate	Fe_2O_3
	Cl	-	Cl salts
	S	Low	SO_3
	Zn	Trace	ZnO
	Mn	Trace	MnO
LSA	K	Low	K_2O
	Ca	High	CaO
	P	-	P_2O_5
	Al	Low	Al_2O_3
	Mg	Low	MgO
	Na	Low	Na_2O
	Fe	Moderate	Fe_2O_3
	Cl	-	Cl salts
	S	Low	SO_3
	Zn	Trace	ZnO
	Mn	Trace	MnO
PSA	K	Low	K_2O
	Ca	High	CaO
	P	-	P_2O_5
	Al	Low	Al_2O_3
	Mg	Low	MgO
	Na	Low	Na_2O
	Fe	Moderate	Fe_2O_3
	Cl	-	Cl salts
	S	Low	SO_3
	Zn	Trace	ZnO
	Mn	Trace	MnO

Fig. 2.b. indicates that the dominant compounds in LSA, SiO_2, CaO, and calcium silicates play a key role in enhancing binder strength and reactivity. Fe_2O_3 contributes to chemical stability and colour, while Al_2O_3 and MgO influence hydration. Minor oxides (K_2O, Na_2O, SO_3) may act as accelerators or impurities. The high SiO_2 and CaO content confirms LSA's strong pozzolanic potential, comparable to established SCMs like rice husk ash and volcanic ash. The LSA binder is primarily composed of SiO_2 and CaO, with notable levels of Fe_2O_3 contributing to thermal stability and influencing reactivity and color. Minor oxides (K_2O, Na_2O, MgO, Al_2O_3, SO_3) affect hydration kinetics and phase stability. This composition highlights LSA's strong pozzolanic potential for binder applications. Elemental analysis was performed using a RIGAKU Supermini200 Sequential WDXRF Spectrometer (Japan). Fig. 2.c. confirms the presence of Al_2O_3 and MgO, indicating their role in hydration and secondary phase formation. Minor elements (Na, K, Zn, Cr, P, S) may influence early geopolymer, phase stability, and durability. PSA mainly consists of SiO_2 and CaO, along with significant amounts of Fe_2O_3, Al_2O_3, and MgO. This highlights its potential as a pozzolanic precursor that can promote C–A–S–H formation and improve early strength development.

2.2. Material Characterization

Material characterization was performed using FTIR to detect functional groups (O–H, C–H, N–A–S–H gels), XRD to examine crystalline phases like C–A–S–H, quartz, kaolin, and zeolite, and SEM to evaluate the microstructure, including porosity, matrix bonding, and morphology. Compressive strength results were analyzed statistically to assess the effect of SF content. FTIR and XRD spectra were analyzed by comparing peaks with reference databases, while SEM images were visually examined in relation to microstructural density and mechanical properties [36].

2.2.1. FTIR

FTIR characterization identifies functional groups in a sample to determine surface chemical composition or molecular structure changes after treatment, activation, heating, or mixing of materials). FTIR spectroscopy works on the principle that chemical bonds in molecules will absorb infrared waves at a specific frequency that corresponds to strain or bend vibrations (vibrations) [36]. Each functional group has a distinctive absorption region, thus allowing identification through the spectrum. The instrument used in this analysis is the Thermal Scientific Nicolet iS10 FTIR Spectrometer, Perkins. preparation solid sample (fine powder). The solvent used is KBr (potassium bromide) with a ratio of 1:10.

2.2.2. XRD

XRD is a non-invasive technique used to analyze the crystal structure of solid materials [37]. This approach uses the interaction of X-rays and atomic lattices in crystalline materials to determine mineral phases, crystallite size, residual stress, and crystalline levels [39]. Sample preparation conducted to produce a smooth, homogeneous, and moisture-free powder surface resulting in a clear, defined, and representative X-ray diffraction pattern (diffractogram) of the crystal structure of the material analyze. Mortar and pestle (porcelain or agate) to fine-tune the sample after it has filtered using a sieve/sieve (usually 75μm or No. 200).

2.2.3. SEM

SEM analysis aims to explore the surface morphology and microstructural features of geopolymer mortars, including the qualitative identification of pores, microcracks, interparticle bonds, and the distribution of phases involved in the polymerization reaction [40,41]. The apparatus utilized comprises the Scanning Electron Microscope JEOL JSM-6510, FEI Hitachi. Sample preparation involves extracting small fragments of geopolymer mortar (about 1 cm^3) from the interior of the test specimen to prevent contamination of the external surface. Dehydrate the sample in the oven at around 60–80°C for a minimum of 24 hours. Determine the geopolymer matrix N–A–S–H or C–A–S–H synthesis.

2.3. Mix Design and Specimen Preparation

The study used LSA, PSA, and RHA as primary pozzolanic precursors, chosen for their high CaO and SiO_2 content. SF was added as a supplementary binder to enhance geopolymer. The alkaline activator consisted of 6 M NaOH and 2.65 M Na_2SiO_3, while a 1% by weight superplasticizer (SP) was included to improve workability, with additional water added as needed for consistency.

The mortar preparation process involved sieving LSA, PSA, RHA, and SF through a 75 µm mesh to ensure uniform particle size. A 6 M NaOH solution was prepared as the alkaline activator, left at room temperature for 24 hours, and then mixed with Na_2SiO_3 in a 1:1 volume ratio. The dry precursors (LSA + SF) were thoroughly blended before gradually adding the alkaline solution, followed by the incorporation of the superplasticizer. The mixtures were poured into 5×5×5 cm molds, cured at 60°C for 48 hours, and then stored at room temperature until day 28, when compressive strength testing was carried out according to ASTM C109/C109M standards [42,43].

In the study, geopolymer mortars were produced using pozzolanic raw materials rich in silica and alumina, such as RHA, PSA, and LSA. The alkaline activator consisted of a combination of NaOH and Na_2SiO_3 with a 1:1 molar ratio, which has been proven to produce the best performance in forming stable and strong geopolymers.

The selection of the 1:1 NaOH to Na_2SiO_3 ratio is based on its ability to efficiently Activate the silica and alumina elements in the raw materials, while ensuring that sufficient silicate is available to form a robust aluminosilicate network. This ratio ensures an optimal balance between reaction rate and geopolymer gel formation, which is crucial for obtaining mortar with good mechanical strength and long-term stability.

Previous studies have shown that the 1:1 NaOH to Na_2SiO_3 ratio is highly effective in improving the mechanical properties of geopolymers. For instance, [44] it was shown that this ratio achieved the highest compressive strength of up to 25.56 MPa after 7 days of curing in geopolymer mortar containing fly ash. Similarly, [35] found that this ratio played a significant role in the formation of a strong aluminosilicate network, contributing to improved mechanical properties of magnesium silicate-based geopolymers. Additionally, [45] Validated the choice of the 1:1 ratio, as their study demonstrated that this ratio enhanced compressive strength in geopolymer mortars derived from different ash sources, such as RHA and PSA.

The 1:1 NaOH to Na_2SiO_3 ratio improves compressive strength and speeds up the formation of the geopolymer network, which has a notable effect on the material's physical and microstructural properties. As a result, this ratio was selected for the study to optimize the performance of producing robust and durable geopolymer mortars.

Table 2. Mix design mortar based on binder for 1 m^3.

Materials	Silica Fume Addition Percentage				
	0%	5%	10%	15%	20%
Water (kg)	105.00	105.00	105.00	105.00	105.00
Super plasticizer (kg)	3.50	3.50	3.50	3.50	3.50
Natrium Silicate Solution (kg)	79.99	79.99	79.99	79.99	79.99
NaOH Solution (kg)	53.33	53.33	53.33	53.33	53.33
Fine Aggregate (kg)	1,500.00	1,500.00	1,500.00	1,500.00	1,500.00
Silica Fume (kg)	0.00	17.50	35.00	52.50	60.00
Binder (kg)	350.00	350.00	350.00	350.00	350.00

Table 2 presents the mix design, which incorporated silica fume (SF) at 5%, 10%, 15%, and 20% of the total precursor weight (LSA + SF). The alkaline activator solution was mixed at a NaOH to Na_2SiO_3 volumetric ratio of 1:1. The binder system consisted of a blend of Lokan shell ash (LSA) and SF, with a 1% superplasticizer by precursor weight to improve workability.

Figure 3 illustrates the procedure for assessing the compressive strength of geopolymer mortar, in accordance with standardized testing protocols. The process involves a sequence of essential steps to guarantee consistent, precise, and dependable results when measuring the compressive strength of geopolymer mortar samples. The samples should be prepared by mixing the specified composition, using the correct proportions of precursor materials (such as fly ash, rice husk ash, palm shell ash, etc.) and alkaline activators such as NaOH and Na_2SiO_3.

The mortar mixture is cast into standardized moulds, typically in a cube shape, such as 50 mm x 50 mm x 50 mm. Ensure that the mortar is well-compacted to eliminate air bubbles. This may be done manually or using a vibrating table. After filling the moulds, the samples should be left to cure in a controlled environment. The curing temperature and duration should follow standard procedures or be adjusted according to the specific needs of the experiment. Once the curing process is complete, the samples are taken out of the moulds and kept under standard conditions until they are ready for testing. The dimensions of the cured samples are measured to ensure they meet the required specifications.

The prepared mortar samples are placed in the TESTMASK testing machine for compressive strength testing. TESTMASK is a mechanical testing machine commonly used for such evaluations, manufactured in Turkey. It is calibrated according to the manufacturer's specifications to ensure accurate results. The samples are placed centrally on the compression platen of the testing machine, ensuring that they are aligned properly to avoid skewed loading during the test. The

testing machine gradually applies compressive force to the sample until it fails, meaning it fractures or breaks apart. The highest load the sample endures before failure is recorded as its compressive strength. Figure 3. illustrates the procedure for Evaluating the compressive strength of geopolymer mortar in accordance with standardized testing procedures. The mechanical tests were conducted using a TESTMASK testing machine, produced in Turkey [42,48].

Fig. 3. Compressive strength testing [34,46,47]

3. Results and Discussion

3.1. Compressive Strength of Geopolymer Mortar

Figure 4 shows the GMPSA, the highest performance in each variation of the addition of silica fume. The compressive strength increases significantly from about 19 MPa (0%) to more than 52 MPa (20%). PSA is highly reactive in geopolymer systems and forms strong bonds with fume silica. The GMPSA demonstrates superior performance compared to GMLSA, although it remains below the standard set by GMRHA. The compressive strength increases from about 13 MPa to almost 47 MPa at 20% silica fume. This indicates that slag has good pozzolan potential but is not as optimal as rice husk ash. GMLSA indicates the lowest compressive strength value among the three. From about 16 MPa (0%) to about 45 MPa (20%). Despite consistent improvements, LSA is less effective than other materials in forming solid geopolymer structures.

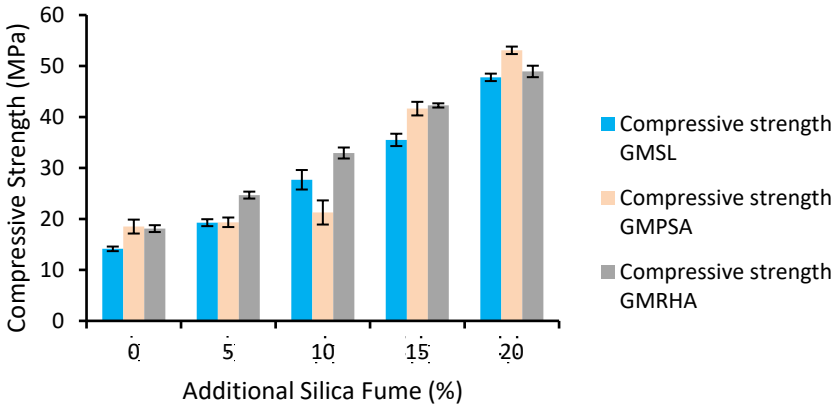

Fig. 4. Compressive strength geopolymer mortar

The incorporation of Silica Fume, varying from 0% to 10%, leads to a gradual increase in compressive strength, though the improvement is not markedly significant. This suggests that the initial activation process and the early development of the N-A-S-H structure have not been fully optimized. However, when SF is added in amounts ranging from 10% to 20%, a significant rise in

compressive strength is observed, emphasizing the crucial role of silica fume in promoting the polycondensation reaction. Silica fume serves as a highly reactive silica source, accelerating the chemical bonding within the geopolymer paste. The maximum effect is observed at 20%, where silica reactivity and bond structure formation reach their peak.

The technical discussion highlights that palm shell ash (PSA) exhibits the highest reactivity due to its high amorphous silica content, which strengthens aluminosilicate bonds. GMSL utilizes the CaO in slag to form C-S-H gel but shows lower microstructural density compared to GMRHA. GMPSA exhibits slower reactivity due to its lower calcium content. Silica fume improves viscosity and microstructural density by filling pores and gaps between particles, leading to denser structures and higher compressive strength. The optimal efficiency is achieved with 15–20% silica fume, avoiding risks of overdosing or segregation.

3.2. Characterization and Morphology of Geopolymer Mortar

Figure 5. illustrates the analysis of crystalline and amorphous phases in LSA-based geopolymer mortar (Lokan Shell Ash/LSA) with the incorporation of silica fume, conducted via X-Ray Diffraction (XRD) technology. The XRD spectrum exhibits a five-stage profile: raw data (Profile), smoothing results (Smoothing Profile), background reduction (B.G. Subtract Profile), Kα1 signal separation, and peak detection (Peak). The five processes demonstrate that the data processing has conducted thoroughly to guarantee precision in the interpretation of the crystalline phase.

Analysis of diffraction peaks revealed the presence of predominant crystalline phases at angles of 2θ approximately 26.6°, 30.1°, 32–34°, and 47–50°. According to the JCPDS database [49–51], the phases included are quartz (Si_2O_2), calcite ($CaCO_3$), and portlandite ($Ca(OH)_2$). Quartz derived from silica remnants in Lokan shell ash and the incorporation of fume silica, whereas calcite and portlandite signify the byproducts of the original reaction between calcium and an alkaline solution. Albite generated through the polymerization of silica and alumina inside a geopolymer framework.

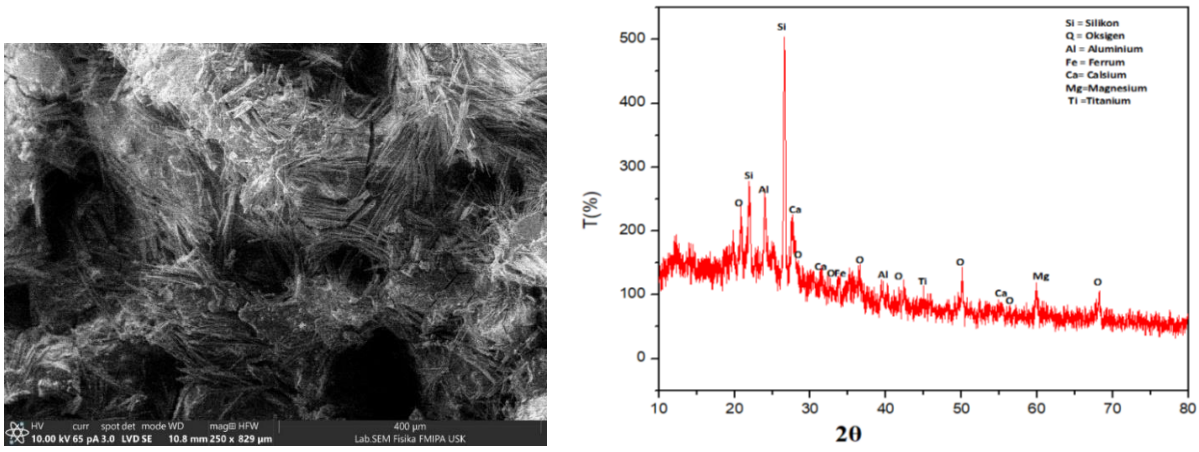

(a) (b)

Fig. 5. (a) SEM and (b) XRD of LSA-based geopolymer mortar

The background spectrum shows a broad peak between 20° and 35°, indicating the dominance of the amorphous N–A–S–H (sodium alumina-silicate hydrate) geopolymer gel phase. This phase lacks sharp peaks due to its irregular structure but contributes to the material's mechanical strength. The incorporation of silica fume promotes the formation of N–A–S–H gels, leading to a more compact and denser microstructure, as indicated by reduced noise and higher intensity in the angular range. Overall, the XRD results indicate that LSA-based geopolymer systems with silica fume addition possess a complex structure, comprising a blend of amorphous phases and small amounts of crystalline material. This provides important mechanical advantages and chemical resistance in environmentally friendly building material applications.

Figure 5 illustrates the mineralogical and microstructural characteristics of geopolymer mortar containing Lokan Shell Ash (LSA). The X-ray diffraction (XRD) pattern displays a notable peak around 29° (2θ), which is attributed to calcite ($CaCO_3$), which confirms the significant calcium carbonate content characteristic of marine shell-based precursors. Additional peaks within the 30°–35° range indicate the presence of portlandite ($Ca(OH)_2$) and gehlenite ($Ca_2Al(AlSi)O_7$), compounds commonly formed in alkali-activated systems as a result of calcium-rich reactions. A wide amorphous peak between 20° and 35° suggests the formation of amorphous aluminosilicate gels, mainly C–A–S–H, which are crucial for the early development of strength. This mixed-phase composition comprising both crystalline and amorphous phases demonstrates that the geopolymerization process proceeded successfully, although the presence of unreacted minerals implies incomplete reaction or limited precursor reactivity.

The SEM micrograph reveals needle- and rod-like crystalline structures, indicative of calcium silicate or ettringite-like formations resulting from the high CaO content in LSA. These morphologies are typically associated with fast-setting behavior and localized crystallization. Regions exhibiting fibrous textures and porous zones reflect areas of intense reaction activity, while the presence of micro-voids and cavities suggests a partially dense matrix. These voids may influence the mechanical properties by reducing density but can also promote inter-particle bonding during curing, The results of the following research as a comparison of research [19,37,43,49,51,52]. Overall, the microstructure demonstrates good initial gel formation and mechanical development; however, heterogeneity in gel distribution and porosity suggests that further optimization of mix design or heat treatment conditions is needed to enhance uniformity and long-term performance.

Table 3. Composition of the main compounds in GMLSA SF20%

Position 2θ (degree)	Chemical compound	Chemical formula	Additional Details
26.6°	Quartz	SiO_2	Silica content from ash
30.1°	Calcite	$CaCO_3$	Ca–Al silicate-forming reactants/fillers
32.0–34.0°	Portlandite	$Ca(OH)_2$	Leftover hydration products or additives
28.0–29.5°	Albite	$NaAlSi_3O_8$	Common aluminosilicates in geopolymerization
47–50°	Hematite/ Magnetite	Fe_2O_3/ Fe_3O_4	Iron content from ash or additives
22–24°	Amorphous hump	-	Indicates the amorphous phase of the geopolymer (general)

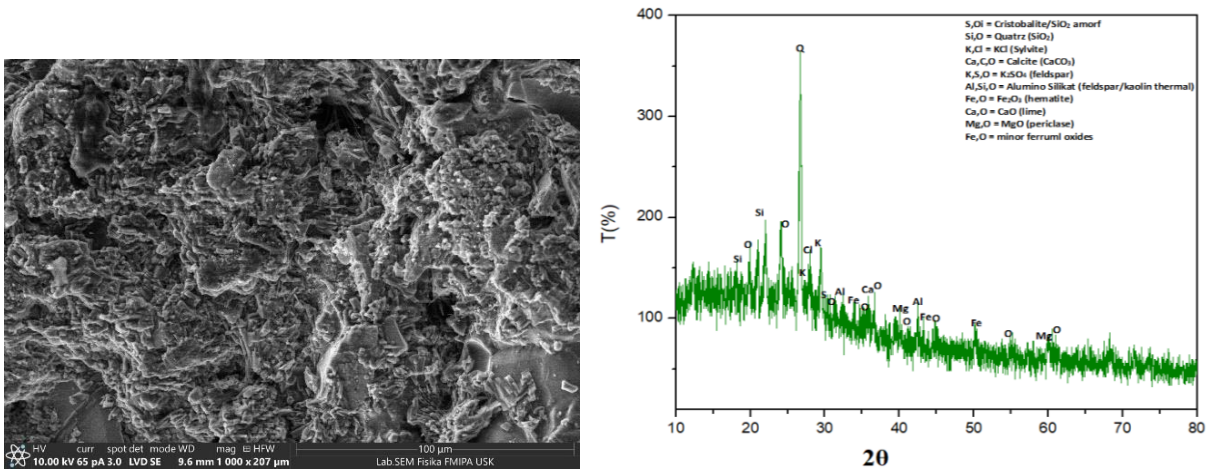

(a) (b)

Fig. 6. (a) SEM and (b) XRD of PSA-based geopolymer mortar

Figure 6. presents the XRD pattern of PSA-based geopolymer mortar, covering a 2θ angle range from 10° to 80°. A prominent peak around 2θ ≈ 27–30° signifies the presence of a crystalline phase, likely silica (SiO_2) or aluminosilicates, which have not fully reacted during the geopolymerization process. The gradual decline in the background pattern suggests the predominance of an amorphous phase, a typical characteristic of geopolymer materials, particularly when alkaline activation has successfully converted early crystalline phases into amorphous aluminosilicate gels (N-A-S-H gels). he strong peak at the primary crest suggests the possible presence of residual crystalline materials from the palm shell ash, including quartz, calcite, or other mineral phases that are resistant to alkaline solutions. In general, the palm shell ash-based geopolymer mortar displays a semi-crystalline structure, with the material in an amorphous state, indicating favorable conditions for geopolymer formation. The distinctness of the peaks suggests that additional optimization is required for complete activation, which could involve increasing the molarity of the alkaline solution, adjusting the Si/Al ratio, or extending the curing time.

Table 4. Composition of the main compounds in GMPSA SF20%

Position 2θ (degrees)	Chemical compound	Chemical formula	Additional Details
26.6°	Quartz (Silika)	SiO_2	Common of silica ash
30.0°	Calcite	$CaCO_3$	Source of calcium
32.0°	Portlandite	$Ca(OH)_2$	Hydration results
33–35°	Albite	$NaAlSi_3O_8$	Alumina-silicate phase
40–50°	Hematite	Fe_2O_3	Iron content from ash
28.0°, ~48.0°	Gehlenite	$Ca_2Al(AlSi)O_7$	General products of geopolymerization

Figure 7. shows a porous surface with small cracks, which suggests that the curing process may be imperfect or too fast. There are large voids and incompact structures, indicating that rice husk ash particles have not fully dispersed or reacted. Such structures can decrease compressive strength and increase porosity, which influences the durability and permeability of the mortar. Large or non-uniform RHA particle sizes. Less homogeneous mixing. Alkaline activation is not optimal if the molarity of the NaOH solution is too low or the Si/Al ratio is not ideal. Lack of curing time or too low curing temperature. The Table 6. presents the compounds formed during the polymerization process in geopolymer mortar made from rice husk ash, with the inclusion of 20% silica fume.

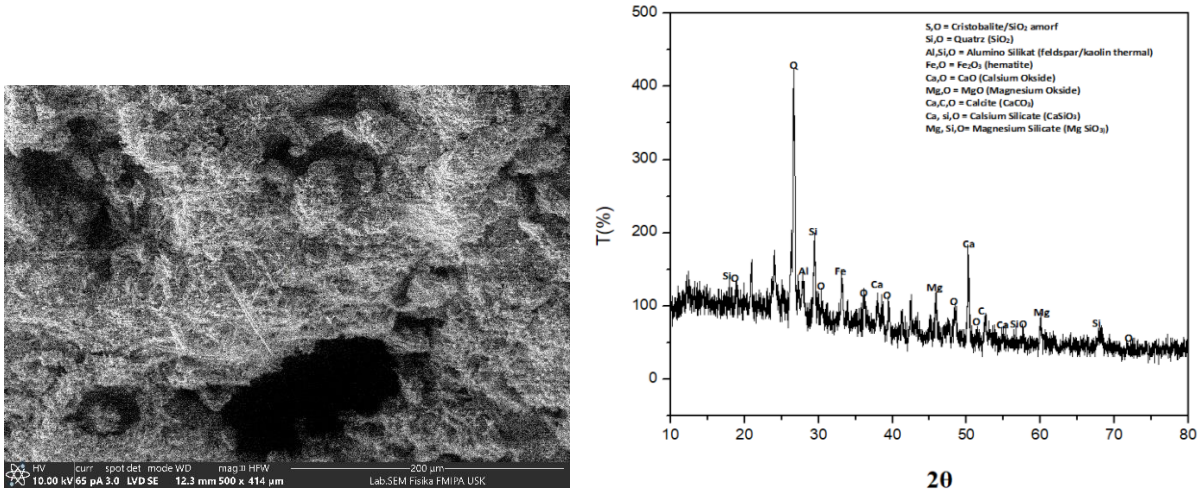

Fig. 7. (a) SEM and (b) XRD of RHA-based geopolymer mortar

Figure 7 displays the dominant diffraction peak around 26.6° (2θ), indicating the presence of quartz (SiO_2). The occurrence of rice husk ash (RHA) is commonly observed, particularly when it has not undergone optimal thermal activation. The absence of a well-defined peak structure, coupled with

a sloping baseline, signifies the predominance of the amorphous phase, which is attributed to the geopolymer gel (N-A-S-H) formed during the polymerization process. Minor peaks observed around 30°–35°, 48°, and 50° suggest the potential presence of compounds such as gehlenite, and hematite, which may either originate from the initial materials or form as reaction by-products. The structure of these RHA-based geopolymers is semi-crystalline, with the amorphous phase being dominant, as expected in successful polymerization. The continued presence of crystalline quartz suggests incomplete dissolution or reaction of the silica in RHA, potentially due to the large particle size or inadequate curing time. The compounds present in geopolymer mortar derived from rice husk ash are summarized in Table 7.

Table 5. Composition of the main compounds in GMRHA SF20%

Position 2θ (degrees)	Chemical compound	Chemical formula	Additional Details
26.6°	Quartz (Silika)	SiO_2	Common of silica ash
30.0°	Calcite	$CaCO_3$	Source of calcium
32.0°	Portlandite	$Ca(OH)_2$	Hydration results
33–35°	Albite	$NaAlSi_3O_8$	Alumina-silicate phase
40–50°	Hematite	Fe_2O_3	Iron content from ash
28.0°, ~48.0°	Gehlenite	$Ca_2Al(AlSi)O_7$	General products of geopolymerization

3.3. FTIR Result of Geopolymer Mortar

Figure 8 presents the Spectrum Zone Analysis and Chemical Interpretation within the 3300–3700 cm^{-1} range (O–H stretching group). Sharp peaks in this region suggest the presence of hydroxyl groups (O-H), which result from both bound water and geopolymer polycondensation reactions. As the silica fume (SF) content increases, the intensity of the O–H peak increases and shifts slightly, indicating the formation of a more active N-A-S-H gel. This change is attributed to the reaction between silica fume and alumina, which boosts the chemical reactivity and development of the gel structure. In the 2800–3000 cm^{-1} range (C–H stretching group), the weak peak suggests traces of residual organic compounds from biomass ash. Although C–H interactions play a minor role in geopolymer network formation, they indicate carbon residue interactions. In the 1000–1200 cm^{-1} range (Si–O–T stretching group; T = Si/Al), a peak shift to a higher frequency with SF addition signals a more condensed silicate-aluminosilicate network. The GMSL spectrum with 20% SF shows the narrowest and strongest peaks, supporting the hypothesis that SF enhances polymerization. Additionally, the 1650–1450 cm^{-1} range (H–O–H bending/structural water deposits) correlates with water trapped within the geopolymer matrix. The addition of SF results in microstructural compaction and reduced porosity.

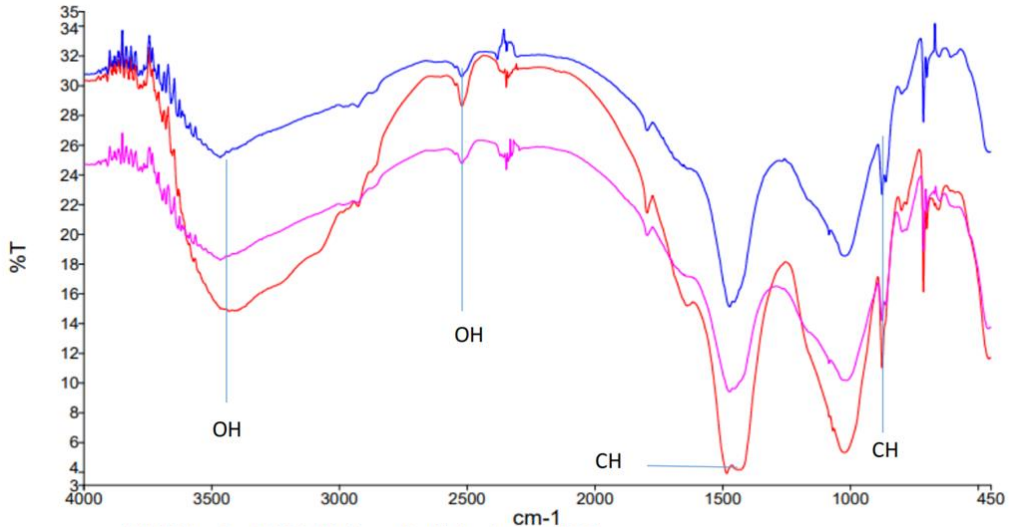

Fig. 8. FTIR test results of LSA-based geopolymer mortar

Figure 9 shows a region at 3400 cm^{-1}, corresponding to O-H stretching, which represents the vibrations of hydroxyl groups, possibly from free water or silicate structures. The intensity of this band decreases as the palm shell ash content increases, suggesting a reduction in free water or stronger hydrogen bonding, both indicating ongoing polymerization. The peak at 2920 cm^{-1}, associated with C-H stretching, reflects organic impurities or carbon residues, with higher intensity observed in samples with higher palm shell ash content (15–20%). The band at 1650 cm^{-1} corresponds to H–O–H bending, further indicating the presence of structural water. Changes in the shape or position of the peak suggest reorganization within the silica-alumina network.

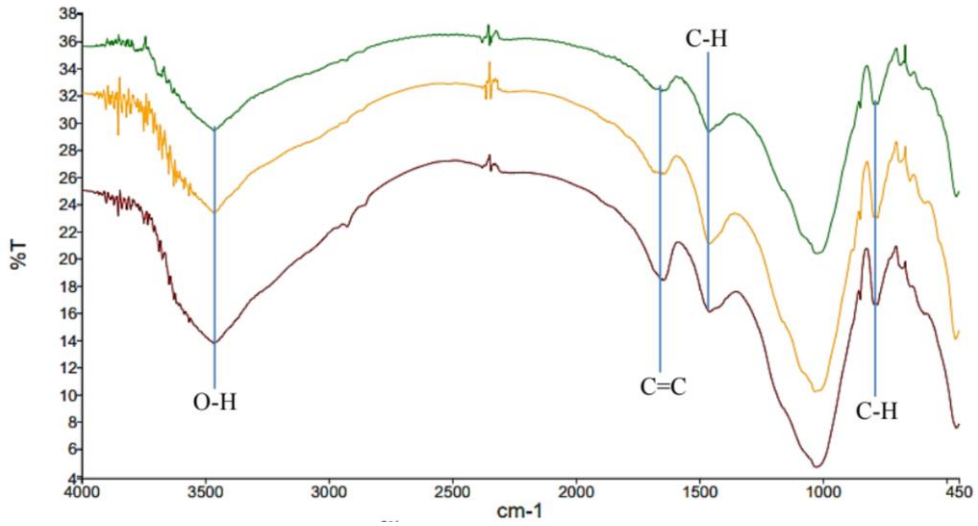

Fig. 9. FTIR test results of PSA-based geopolymer mortar

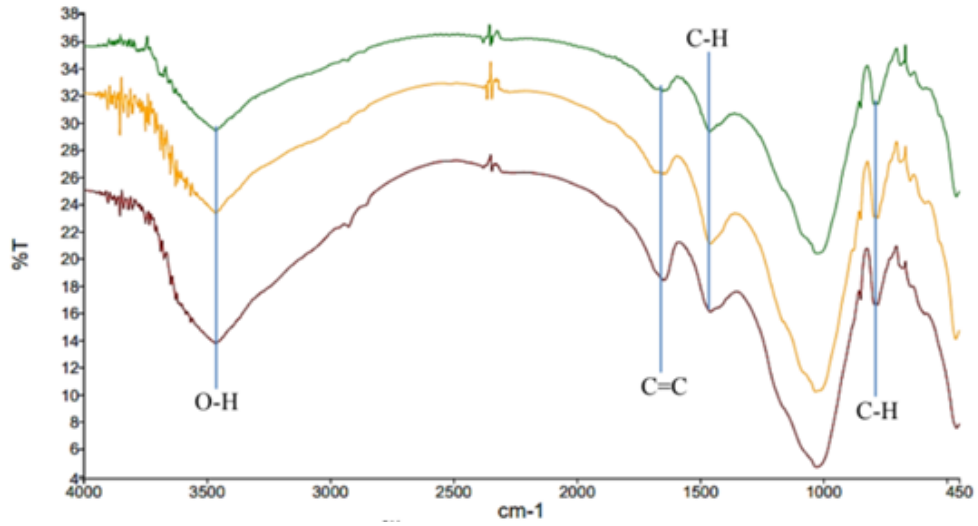

Fig.10. FTIR test results of RHA-based geopolymer mortar

The 1000–1100 cm^{-1} region corresponds to the asymmetric stretching of Si–O–T (where T is Si or Al) in geopolymer structures. For ash additions of 10–15%, the bands show a distinct profile and a slight shift to lower wavenumbers, indicating increased condensation and polymerization rates. At 20% ash content, the band broadens, suggesting potential disruption of the silica-alumina gel network due to an excess of ash. The band in the 875–700 cm^{-1} range, corresponding to bending vibrations of C–H or Si–O–Al, shows increased intensity in samples with 15–20% ash, potentially due to the influence of carbon structures in the ash on the geopolymer network. As shown in Figure 10, an increase in the C–H band reflects the organic influence of palm shell ash, which may either positively impact the structure (by densifying the matrix) or negatively affect the polycondensation process. Adding 10–15% palm shell ash leads to sharper Si–O–T bands, indicative of a more active polymerization reaction. At 20% ash content, the spectra suggest potential saturation or disruption

of reactions, likely due to the excess carbon or acid material, which may hinder the polycondensation process. The reduction in the O–H band and shift observed in the Si–O band further suggest enhanced silicate condensation, resulting in more robust aluminosilicate structures.

The increase in compressive strength with rising silica fume (SF) content is directly associated with the enhanced formation of geo-polymeric gels, particularly sodium aluminosilicate hydrate (N-A-S-H) and calcium-aluminosilicate hydrate (C-A-S-H), which contribute to matrix densification and improved mechanical properties. The fine particle size and high pozzolanic reactivity of SF supplied additional soluble silica, promoting the dissolution of aluminosilicate species and accelerating geopolymerization. PSA-based mortars demonstrated the highest strength values, especially at 20% SF, due to the balanced chemical composition that supported a more complete and homogeneous gel network. In contrast, RHA mortars, while rich in silica, lacked sufficient alumina for optimal network formation, and LSA mortars, with their higher calcium content, exhibited heterogeneous structures with residual crystalline phases and microcracks. These trends are supported by microstructural analyses: XRD confirmed the predominance of amorphous phases, with broad humps between 20°–35° 2θ; FTIR spectra revealed intensified Si–O–T and O–H bond vibrations with increasing SF, indicating better gel development and reduced porosity; and SEM images showed denser matrices in PSA mortars, while LSA samples displayed porous and irregular microstructures. Together, these results confirm the synergistic role of SF in refining the microstructure and enhancing the mechanical performance of geopolymer mortars. It is further recommended to present compressive strength results with standard deviation and error bars to improve statistical clarity. Overall, the integration of SF with biomass-based precursors, especially PSA, demonstrates significant potential for developing high-strength, durable, and eco-friendly geopolymer composites suitable for sustainable construction applications.

4. Conclusion

The study provides a detailed investigation into the role of silica fume (SF) in enhancing the mechanical and microstructural properties of geopolymer mortars derived from biomass-based precursors—namely rice husk ash (RHA), palm shell ash (PSA), and lokan soil ash (LSA). The use of SF at various substitution levels (0%, 5%, 10%, 15%, and 20% by binder weight) allowed for a comprehensive assessment of its influence on strength development and internal structure. Among the three systems, PSA-based mortars exhibited the most significant improvement in compressive strength, reaching up to 52 MPa at 20% SF, highlighting the synergistic effect between the precursor and the reactive silica from SF. This enhancement is primarily attributed to the refined microstructure and accelerated geopolymerization process induced by SF addition.

Microstructural characterizations provided strong evidence supporting the mechanical results. XRD analysis confirmed the dominance of amorphous phases in all geopolymer matrices, indicating successful geopolymerization, with wide humps around 20°–35° 2θ representing the formation of sodium aluminosilicate hydrate (N-A-S-H) and, in some LSA mortars, calcium-aluminosilicate hydrate (C-A-S-H) gels. Minor crystalline phases such as quartz and calcite were detected in PSA and LSA mortars, likely due to the presence of unreacted components. SEM observations revealed notable differences in microstructure across systems, with RHA mortars showing denser and more homogeneous surfaces, whereas LSA mortars exhibited visible needle-like crystalline formations and higher porosity. FTIR spectra supported these observations, showing intensified Si–O–T and O–H bond vibrations in mortars with higher SF content, suggesting improved gel formation and lower internal porosity.

The optimal performance of geopolymer mortars was observed when SF was incorporated at 10–20% by weight. Within this range, the mortars demonstrated a desirable balance between mechanical strength, workability, and microstructural uniformity. The high surface area and pozzolanic reactivity of SF enhanced the dissolution of precursor materials and the subsequent polymerization reactions, resulting in better-integrated binder matrices. Lower SF contents failed to achieve this level of enhancement, while excessively high SF could affect mix workability.

In conclusion, the integration of silica fume into biomass-based geopolymer mortars significantly improves both strength and durability, particularly in systems utilizing PSA. The results reinforce the potential of agro-industrial and marine waste materials as viable precursors for sustainable binder systems, with SF acting as a key performance enhancer. These findings contribute to the growing body of knowledge on eco-efficient construction materials and suggest practical applications in producing high-strength, durable, and environmentally responsible geopolymer mortars. Future studies may focus on long-term durability, shrinkage behavior, and large-scale applicability to fully realize the potential of these hybrid systems in structural and infrastructure applications.

Acknowledgement

This study was funded by the Direktorat Penelitian dan Pengabdian kepada Masyarakat, Direktorat Jenderal Litbang dan Pengembangan, Kementerian Pendidikan Tinggi, Ilmu Pengetahuan, dan Teknologi (Contract No. 117/C3/DT.05.00/PL/2025), and the Institute for Research and Community Service, Universitas Teuku Umar, under the Fundamental Regular Research Scheme (Contract No. 18/UN59.L1/AL.04/PL/2025), which supported the provision of palm shell ash and silica fume. We also acknowledge the Laboratories of Materials and Mineral Processing at Universitas Teuku Umar and Universitas Syiah Kuala for providing access to XRD, FTIR, and SEM facilities. Our sincere thanks go to the research team and technical staff for their invaluable collaboration and support in ensuring the successful completion of this study.

References

[1] Luhar I, Luhar S. A comprehensive review on fly ash-based geopolymer. Journal of Composites Science. 2022;6(8):219. https://doi.org/10.3390/jcs6080219

[2] Singh RP, Vanapalli KR, Cheela VRS, Peddireddy SR, Sharma HB, Mohanty B. Fly ash, GGBS, and silica fume based geopolymer concrete with recycled aggregates: Properties and environmental impacts. Construction and Building Materials. 2023;131168. https://doi.org/10.1016/j.conbuildmat.2023.131168

[3] Maheswaran M, Christy CF, Muthukannan M, et al. Parametric study on the performance of industrial byproducts based geopolymer concrete blended with rice husk ash & nano silica. Research on Engineering Structures and Materials. 2023. http://dx.doi.org/10.17515/resm2023.809ma0703

[4] Hossain SS, Roy PK, Bae CJ. Utilization of waste rice husk ash for sustainable geopolymer: A review. Construction and Building Materials. 2021;310:125218. https://doi.org/10.1016/j.conbuildmat.2021.125218

[5] Freire AL, Moura-Nickel CD, Scaratti G, Rossi AD, Araújo MH, Júnior ADN, et al. Geopolymers produced with fly ash and rice husk ash applied to CO2 capture. Journal of Cleaner Production. 2020;273:122917. https://doi.org/10.1016/j.jclepro.2020.122917

[6] Wang H, Tao Y, Yang X, Liu L, Lin W, Wang M, Qu C. Influence of silica–alumina-modified materials on mechanical properties of fly ash-based geopolymers. International Journal of Geosynthetics and Ground Engineering. 2024;10(2):23. https://doi.org/10.1007/s40891-024-00532-8

[7] Marcos KD, Calamba MG, Mores AJ Jr. Optimization of geopolymer concrete using fly ash, rice husk ash, and coconut shell ash for improved workability, durability and mechanical performance using response surface methodology. In: International Conference on Civil Engineering. Springer; 2025. p.3–13. https://doi.org/10.1007/978-981-96-8990-3_1

[8] Alaneme GU, Olonade KA, Esenogho E. Eco-friendly agro-waste based geopolymer-concrete: a systematic review. Discover Materials. 2023;3(1):14. https://doi.org/10.1007/s43939-023-00052-8

[9] Singh S, Aswath MU, TB S. Effect of silica on the properties of red mud based geopolymer mortar for synthesis of sustainable bricks. Journal of Building Pathology and Rehabilitation. 2024;9(1):67. https://doi.org/10.1007/s41024-024-00424-4

[10] Konduru H, Karthiyaini S, Shanmugasundaram M. Comparative study of silica fume and sodium silicate as replacement of active reactive silica in bauxite residue based geopolymer mortar. Case Studies in Construction Materials. 2025;22:e04302. https://doi.org/10.1016/j.cscm.2025.e04302

[11] Ashkan H, Norhisham S, Abu Bakar MS, Syamsir A, Abdullah MJ, Muhammad Asyraf MR, et al. The mechanical performance of polymer concrete incorporating waste tin fibres. Pertanika Journal of Science & Technology. 2024;32(1). http://www.pertanika.upm.edu.my/resources/files/Pertanika%20PAPERS/JST

[12] Ogwang G, Olupot PW, Kasedde H, Menya E, Storz H, Kiros Y. Experimental evaluation of rice husk ash for applications in geopolymer mortars. Journal of Bioresources and Bioproducts. 2021;6(2):160–7. https://doi.org/10.1016/j.jobab.2021.02.008

[13] Ranjbar N, Mehrali M, Behnia A, Alengaram UJ, Jumaat MZ. Compressive strength and microstructural analysis of fly ash/palm oil fuel ash based geopolymer mortar. Materials & Design. 2014;59:532–9. https://doi.org/10.1016/j.matdes.2014.03.037
[14] Abdullah NO, Bachtiar RDW, Rusni NK. A sustainable environmental study on clamshell powder, slag, bagasse ash, fly ash, and corn cob ash as alternative cementitious binder. In: IOP Conference Series: Earth and Environmental Science. IOP Publishing; 2021. p.012003. https://doi.org/10.1088/1755-1315/841/1/012003
[15] Bellum RR, Al Khazaleh M, Pilla RK, Choudhary S, Venkatesh C. Effect of slag on strength, durability and microstructural characteristics of fly ash-based geopolymer concrete. Journal of Building Pathology and Rehabilitation. 2022;7(1):25. https://doi.org/10.1007/s41024-022-00163-4
[16] Khater HM, Gharieb M. Synergetic effect of nano-silica fume for enhancing physico-mechanical properties and thermal behavior of MK-geopolymer composites. Construction and Building Materials. 2022;350:128879. https://doi.org/10.1016/j.conbuildmat.2022.128879
[17] Pan Z, Tan M, Zheng G, Wei L, Tao Z, Hao Y. Effect of silica fume type on rheology and compressive strength of geopolymer mortar. Construction and Building Materials. 2024;430:136488. https://doi.org/10.1016/j.conbuildmat.2024.136488
[18] Wang T, Fan X, Gao C. Strength, pore characteristics, and characterization of fly ash-slag-based geopolymer mortar modified with silica fume. In: Structures. Elsevier; 2024. p.107525. https://doi.org/10.1016/j.istruc.2024.107525
[19] Altawil H, Olgun M. Optimization of mechanical properties of geopolymer mortar based on Class C fly ash and silica fume: A Taguchi method approach. Case Studies in Construction Materials. 2025;22:e04332. https://doi.org/10.1016/j.cscm.2025.e04332
[20] Suwannasingha N, Kantavong A, Tunkijjanukij S, Aenglong C, Liu HB, Klaypradit W. Effect of calcination temperature on structure and characteristics of calcium oxide powder derived from marine shell waste. Journal of Saudi Chemical Society. 2022;26(2):101441. https://doi.org/10.1016/j.jscs.2022.101441
[21] Asbiartha P, Alfa A, Sudeska E. Effect of virgin shells and lokan powder as a partial substitute for cement on the volume, compressive strength and tensile strength of concrete. Selodang Mayang Jurnal Ilmiah. 2022;8(1):48–56. https://doi.org/10.47521/selodangmayang.v8i1.246
[22] Janarthanan K, Sivanandi P. Extraction and characterization of waste plastic pyrolysis oil for diesel engines. Journal of Cleaner Production. 2022;366:132924. https://doi.org/10.1016/j.jclepro.2022.132924
[23] Mashri MOM, Megat Johari MA, Ahmad ZA, Mijarsh MJA. Influence of milling process of palm oil fuel ash on the properties of palm oil fuel ash-based alkali activated mortar. Case Studies in Construction Materials. 2022;16:e00857. https://doi.org/10.1016/j.cscm.2021.e00857
[24] Rasid NNA, Khalid NHA, Mohamed A, Sam ARM, Majid ZA, Huseien GF. Ground palm oil fuel ash and calcined eggshell powder as SiO2–CaO based accelerator in green concrete. Journal of Building Engineering. 2023;65:105617. https://doi.org/10.1016/j.jobe.2022.105617
[25] Adeleke BO, Kinuthia JM, Oti J, Ebailila M. Physico-mechanical evaluation of geopolymer concrete activated by sodium hydroxide and silica fume-synthesised sodium silicate solution. Materials. 2023;16(6):2400. https://www.mdpi.com/1996-1944/16/6/2400
[26] Wu Y, Lu B, Bai T, Wang H, Du F, Zhang Y, et al. Geopolymer, green alkali activated cementitious material: Synthesis, applications and challenges. Constr Build Mater. 2019;224:930–49. https://doi.org/10.1016/j.conbuildmat.2019.07.112
[27] Assi LN, Carter K, Deaver E, Ziehl P. Review of availability of source materials for geopolymer/sustainable concrete. J Clean Prod. 2020;263:121477. https://doi.org/10.1016/j.jclepro.2020.121477
[28] Öz HÖ, Doğan-Sağlamtimur N, Bilgil A, Tamer A, Günaydin K. Process development of fly ash-based geopolymer mortars in view of the mechanical characteristics. Materials. 2021;14(11):2935. https://doi.org/10.3390/ma14112935
[29] Salami BA, Bahraq AA, ul Haq MM, Ojelade OA, Taiwo R, Wahab S, et al. Polymer-enhanced concrete: A comprehensive review of innovations and pathways for resilient and sustainable materials. Next Mater. 2024;4:100225. https://doi.org/10.1016/j.nxmate.2024.100225
[30] Balo AM, Rahier H, Mobili A, Katsiki A, Fagel N, Chinje UM, et al. Metakaolin-based inorganic polymer synthesis using cotton shell ash as sole alkaline activator. Constr Build Mater. 2018;191:1011–22. https://doi.org/10.1016/j.conbuildmat.2018.10.047
[31] Yusof M. Mechanical and thermo-physical properties of Polymesoda bengalensis reinforced polymer-matrix composites [thesis]. Kuala Lumpur: University of Malaya; 2018. https://www.proquest.com/openview/d80bd787a769e6ea683c4be9a9f3c356/1
[32] López LCS, Ramos JCL, De La Rosa YEN, Bruschi GJ, Baldovino JDJA. Stabilization of clay soils using a lime derived from seashell. Materials. 2025;18(12):2723. https://doi.org/10.3390/ma18122723

[33] Yusra A, Hasan M, Husin H, Aulia TB. The impact of silica fume addition on early age compressive and flexural strength of geopolymer mortar with various binders. In: Chate VR, Verma A, Tajuddin FN, editors. E3S Web Conf. 2025;621:01007. https://doi.org/10.1051/e3sconf/202562101007
[34] Premkumar R, Ramesh BC, Meyyappan PL, Shanmugasundaram M. Influence of Na_2SiO_3/NaOH ratio on calcined magnesium silicate based geopolymer—Experimental and predictive study. J Wuhan Univ Technol Mater Sci Ed. 2023;38(5):1077–85. https://doi.org/10.1007/s11595-023-2796-z
[35] Zhao Q, Ma C, Lu X, Huang B, Chen Z, Lian C. Effect of silica fume on the efflorescence, strength and micro-properties of one-part geopolymer incorporating sewage sludge ash. Constr. Build Mater. 2024;436:136840. https://doi.org/10.1016/j.conbuildmat.2024.136840
[36] Koczoń P, Hołaj-Krzak JT, Palani BK, Bolewski T, Dąbrowski J, Bartyzel BJ, et al. The analytical possibilities of FT-IR spectroscopy powered by vibrating molecules. Int J Mol Sci. 2023;24(2):1013. https://doi.org/10.3390/ijms24021013
[37] Ali A, Chiang YW, Santos RM. X-ray diffraction techniques for mineral characterization: A review for engineers of the fundamentals, applications, and research directions. Minerals. 2022;12(2):205. https://doi.org/10.3390/min12020205
[38] Lodh A, Thool K, Samajdar I. X-ray diffraction for the determination of residual stress of crystalline material: An overview. Trans Indian Inst Met. 2022;75(4):983–95. https://doi.org/10.1007/s12666-022-02540-6
[39] Kishore K, Sheikh MN, Hadi MN. Doped multi-walled carbon nanotubes and nanoclay based geopolymer concrete: An overview of current knowledge and future research challenges. Cem Concr Compos. 2024;105774. https://doi.org/10.1016/j.cemconcomp.2024.105774
[40] Khalid LWK. Modelling and optimization of fresh and mechanical properties of fiber reinforced geopolymer mortars for utilizing in 3D concrete printing technology [thesis]. 2024. http://hdl.handle.net/11513/4085
[41] Ergeshov Z, Örklemez E, Ketema AF, Kwami MIA, Ilkentapar S, Durak U, et al. Influence of silica fume on the mechanical and microstructural properties and life cycle assessment of fly ash-based geopolymer mortar. Arabian J Sci Eng. 2025. https://doi.org/10.1007/s13369-025-10142-9
[42] Liu Z, Deng P, Zhang Z. Application of silica-rich biomass ash solid waste in geopolymer preparation: A review. Constr Build Mater. 2022;356:129142. https://doi.org/10.1016/j.conbuildmat.2022.129142
[43] Triana D, Allwar A, Winarno S, Teguh M. Utilization of palm kernel shell for fly ash geopolymer mortar in Indonesia. GEOMATE J. 2025;29(133):167–75. https://geomatejournal.com/geomate/article/view/5066
[44] Chowdhurya JA, Islama MS, Islama MA, Al Bari MA, Debnatha AK. Analysis of mechanical properties of fly ash and boiler slag integrated geopolymer composites. Sustain Struct. 2025;5(2):000073. http://www.sustain/
[45] Hasan K, Yahaya FM, Karim A, Othman R. Investigation on the properties of mortar containing palm oil fuel ash and seashell powder as partial cement replacement. Construction. 2021;1(2):50–61. https://doi.org/10.15282/cons.v1i2.6679
[46] Hasan M, Saidi T. Properties of blended cement paste with diatomite from Aceh Province Indonesia. In: IOP Conf Ser Mater Sci Eng. 2020;796:012034. https://iopscience.iop.org/article/10.1088/1757-899X/796/1/012034/meta
[47] Pan Z, Tan M, Zheng G, Wei L, Tao Z, Hao Y. Effect of silica fume type on rheology and compressive strength of geopolymer mortar. Constr Build Mater. 2024;430:136488. https://doi.org/10.1016/j.conbuildmat.2024.136488
[48] Tipcompor N, Thongtem S, Thongtem T. Characterization of cubic $AgSbS_2$ nanostructured flowers synthesized by microwave-assisted refluxing method. J Nanomater. 2013;2013(1):970489. https://doi.org/10.1155/2013/970489
[49] Madarász J, Beregi E, Sztatisz J, Földvári I, Pokol G. Combined DTA and XRD study of sintering steps towards $YAl_3(BO_3)_4$. J Therm Anal Calorim. 2001;64:1059–65. https://doi.org/10.1023/A:1011508021047
[50] Lu W, Shen Y, Xie A, Zhang W. Green synthesis and characterization of superparamagnetic Fe_3O_4 nanoparticles. J Magn Magn Mater. 2010;322(13):1828–33. https://doi.org/10.1016/j.jmmm.2009.12.035
[51] Park S, Yu J, Oh JE, Pyo S. Effect of silica fume on the volume expansion of metakaolin-based geopolymer considering the silicon-to-aluminum molar ratio. Int J Concr Struct Mater. 2022;16(1):20. https://doi.org/10.1186/s40069-022-00510-2
[52] Wang H, Wu H, Xing Z, Wang R, Dai S. The effect of various Si/Al, Na/Al molar ratios and free water on micromorphology and macro-strength of metakaolin-based geopolymer. Materials. 2021;14(14):3845. https://doi.org/10.3390/ma14143845